

Decoherence and dephasing in multilevel systems interacting with thermal environment

T. Hakioglu and Kerim Savran¹

¹Department of Physics, Bilkent University, Bilkent, 06533 Ankara, Turkey

We examine the effect of multilevels on decoherence and dephasing properties of a quantum system consisting of a non-ideal two level subspace, identified as the qubit and a finite set of higher energy levels above this qubit subspace. The whole system is under interaction with an environmental bath through a Caldeira-Leggett type coupling. The model interaction we use can generate nonnegligible couplings between the qubit states and the higher levels upto $N = 10$. In contrast to the pure two-level system, in a multilevel system the quantum information may leak out of the qubit subspace through nonresonant as well as resonant excitations induced by the environment. The decoherence properties of the qubit subspace is examined numerically using the master equation formalism of the system's reduced density matrix. We numerically examine the relaxation and dephasing times as the environmental frequency spectrum, the environmental temperature, and the multilevel system parameters are varied. We observe the influence of all energy scales in the noise spectrum on the short time dynamics implying the dominance of nonresonant transitions at short times. The relaxation and dephasing times calculated, strongly depend on N for $4 < N < 10$ and saturate for $10 < N$. We also examine double degenerate systems with $4 \leq N$ and observe a strong suppression (almost by two orders of magnitude) of the low temperature relaxation and dephasing rates.

An important observation for $4 \leq N$ in doubly degenerate energy configuration is that, we find a strong suppression of the RD rates for such systems relative to the singly degenerate ones. These results are also compared qualitatively with the relaxation rates found from the Fermi Golden Rule.

PACS numbers: 03.65.Xx, 85.25.Cj, 85.25.D-

I. INTRODUCTION

Currently a large number of model approaches are present for formulating the decoherence phenomena in the literature. The original Caldeira-Leggett model¹ is based on a quantum system under the influence of a double well tunneling potential with a linear coupling to an infinite bath of harmonic oscillators. If the potential is sufficiently smooth and the high energy levels are sufficiently above the tunneling barrier this original model is normally represented as a two level system² (2LS) interacting with a bosonic environmental bath (spin-boson model). An incomplete list of this wide literature is provided in^{3,4,5}. Another popular model of decoherence is the central spin system in which central 2LS couples to large number of environmental two level systems. The pros and cons of these two rival models have been extensively studied⁵.

Realistically, and aside from the genuine 2LS, a large majority of physical systems suggested for qubit is far from being ideal. In a quantum computational environment, the parameters of the physical systems are manipulated to perform the gate operations. For instance, in a multilevel system (MLS), short time pulses used in the manipulation of the states in the qubit subspace induce nonresonant transitions out of the qubit subspace. That nonresonant transitions contribute to the decoherence of the quantum system was recently addressed by Tian and Lloyd⁶. They suggest that after these transitions are induced an optimized sequence of controlled pulses can be applied to cancel the nonresonant effects at arbitrary precision. The idea being physically correct, requires an ad-

ditional knitting of error correction which undoubtedly costs computational time. On the other hand, one may address the same issue by seeking for an alternative solution: Can one understand the effect of the higher levels on decoherence in a well-parameterized MLS coupled to an environment?

The MLS can itself be manifestly N -levelled or a truncated approximation of a larger system with much higher number of levels. Well known examples of both cases have been known. For the former, organic molecules with certain discrete rotational symmetries and ground state low temperature configurations of single polymerized chains are good examples. The vibrational energy spectra of atoms and molecules is a good example for the latter.

These type of realistic MLS can be found for instance in already well-examined superconducting systems such as the rf-SQUID in the charge, flux or phase regimes. We remark however, that a concise treatment of the decoherence effects in MLS has not been fully developed. This work is planned to be a modest step forward in that direction.

In section II we give an introduction of the model MLS used in the present work. Here we merely concentrate on the properties of the environmentally induced dipole matrix elements. Section III recalls the reduced density matrix (RDM) master equation formalism and adapts it for the coupling of the MLS to the environment. The noise correlator, which is considered to be in thermal equilibrium, and the system-noise kernel, for which no Markovian assumption is made, are defined in section IIIA. The results are presented together with the ear-

lier observations of the 2LS (in section IIIB) to allow a comparison with some of the established facts. The MLS with three or higher levels are examined in section IIIC separately for $N = 3$, $N = 4$ and $4 < N$. The section IIIC and the following section IV comprise most of the original results of the manuscript. In section IV, the relaxation times for MLS, which we produced numerically in section III, are compared with the estimates found by using the semi-analytic Fermi Golden Rule (FGR).

II. THE MULTILEVEL SYSTEM

In principle the majority of the well established methods (particularly the influence functional) used in the literature automatically accommodate multilevel dynamics. The results are generally hoped to be true for 2LS in the WKB limit at sufficiently low temperatures^{1,2}. Such techniques are also often preferable since they allow explicit analytic expressions for the decoherence times as functions of the system's parameters. On the other hand, exact methods are also available on pure 2LS⁴. However, we need to accommodate in our parameters explicit degeneracy factors as well as the Hilbert space dimensions. For the latter, the influence functional formalism has no parametric dependence. In this work, in order to retain in our calculations the dependence on the system's Hilbert space dimension, we resort to the system's eigenenergy basis representation.

Our MLS model is an rf-SQUID operating in the quantum coherence regime given by the Hamiltonian

$$H_s = (\hbar \omega_0) = \frac{1}{2} [\omega_J^2 + (z \omega_{bias})^2] + \cos(z) \quad (1)$$

where $\omega_0 = 2\pi / LC$ is the harmonic energy with L being the inductance of the SQUID loop and C is the effective capacitance of the Josephson junction, $\omega_J = E_J / \hbar$ is the dimensionless ratio of the Josephson energy E_J to the harmonic energy, $\omega_{bias} = 2\pi \omega_{bias} / \omega_0$ is a dimensionless scale parameter, $\omega_{bias} = 2\pi \omega_{bias} / \omega_0$ is the effective bias in the flux which is applicable in a current bias junction, and $z = 2\pi \Phi / \Phi_0$ is the flux ($\Phi_0 = hc/2e$ is the superconducting flux quantum). Truncating the Hilbert space dimension at N in the energy eigenbasis, the system Hamiltonian in (1) is written in the diagonal form

$$H_s = \sum_{n=0}^{N-1} E_n(f, g) |f, g\rangle \langle f, g| \quad (2)$$

where f, g describes the set of system parameters $\omega_0, \omega_J, \omega_{bias}$ where $E_n(f, g)$, and $|f, g\rangle$ are respectively the parameter dependent eigenenergies and eigenvectors of the MLS. This set of parameters is sufficiently general to accommodate for all possible effects including the degeneracy in the qubit subspace, the symme-

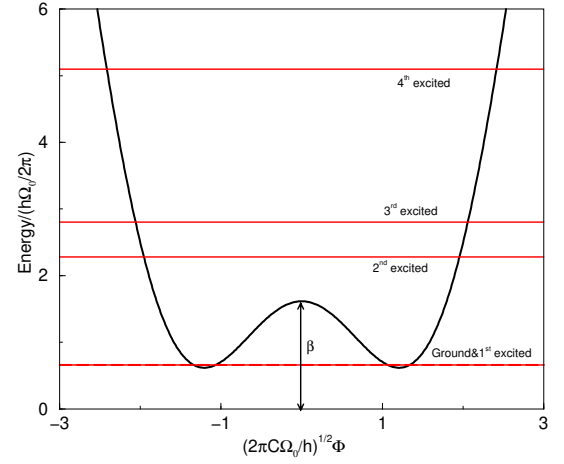


FIG. 1: The double-well potential and the eigenenergy configurations corresponding to the singly degenerate (SD) case. Here the numerical values of the dimensionless parameters for this SD configuration are $\omega_J' = 1.616$ and $\omega_{bias}' = 1.753$. The harmonic energy scale and the degeneracy factors are respectively $\hbar \omega_0 = 10^{-3}$ eV and $\omega_J = 10^6$. Here the numerical values of the dimensionless parameters are $\omega_J' = 1.616$ and $\omega_{bias}' = 1.753$.

try of the wavefunctions etc. [we define the degeneracy factor by $\omega_J = (E_2 - E_1) = (E_1 - E_0)$ for MLS and $\omega_J = (E_1 + E_0) = (E_1 - E_0)$ for 2LS]. These three parameters $\omega_0, \omega_J, \omega_{bias}$ control the high energy harmonic spectrum, the low energy anharmonic spectrum and the reaction symmetry of the rf-SQUID potential respectively. At low energies, a simple numerical diagonalization (1) reveals that there are low lying eigenenergy configurations within the double well regime in which the SQUID potential is strongly anharmonic. The parameters of the potential can therefore be manipulated to search within this regime for those configurations satisfying optimal qubit conditions. An interesting case here is to find highly degenerate⁷ levels corresponding to the first two eigenstates for the symmetric double well potential (i.e. $\omega_{bias} = 0$). This particular case has been extensively examined previously for 2LS using semiclassical methods with an arbitrarily weak tunneling between the wells^{2,3}. Another configuration that turns out to be important in our calculations is the doubly degenerate (DD) configuration for systems with $4 \leq N$ in which the first four levels are pairwise degenerate with large degeneracy factors. The double-well potential and energies corresponding to both SD and DD configurations are shown in Fig's (1) and (2) respectively.

We numerically find that, the relaxation/dephasing (RD) times for the MLS can be controlled by the degeneracy. Normally, degeneracy is also crucial in controlling the dynamical tunneling rates. In our calculations however we directly use the system eigenstates. Therefore for the highly degenerate configurations bare tunneling between symmetric and anti-symmetric parts of the wavefunctions can be neglected to a large extent. This turns

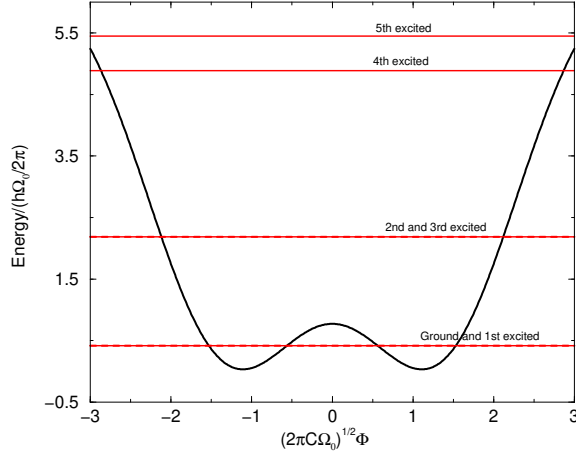


FIG. 2: The double-well potential and the eigenenergy configurations corresponding to the doubly degenerate (DD) case considered throughout the manuscript. The numerical values of the dimensionless parameters corresponding to this DD configuration are $\gamma = 0.772$ and $\beta = 2.187$. The harmonic energy scale and the degeneracy factors are $\hbar\omega_0 = 10^{-3}$ eV, $\gamma_2 = 10^6$; $\gamma_3 = 10^6$.

out to be especially important for quantum computation in the sense that once the computation is finished the wavefunction can be maximally localized in one of the double wells before any measurement or read-out process.

Although we use the truncated rf-SQUID as the N -level model quantum system to study decoherence effects, our treatment is not at the microscopic level. The rf-SQUID is shown to be an ideal model to study multilevel effects due to the fact that, the transitional dipole couplings between the low lying energy states and the high levels are nonnegligible [see Fig. (3)]. Any other physical Hamiltonian with sufficient number of adjustable parameters as well as nonnegligible dipole couplings would be suitable for the calculations presented here.

In the rest of the paper the harmonic energy $\omega_0 = 2\pi/LC$ is a free parameter which is used for scaling energy and time.

A. Coupling to Noise

The system-noise interaction is considered to be a Caldeira-Leggett type inductive coupling between the SQUID's macroscopic flux coordinate z and the environmental flux-like coordinate ϕ_e expanded in harmonic environmental modes as $\phi_e = \sum_k \phi_k (b_k^\dagger + b_k)$. The system-noise interaction is simply $H_{int} = \frac{\gamma}{2} z \phi_e$ where γ is some number representing the strength of the inductive coupling (γ is to be normalized by ω_0 for a dimensionless coupling). In the diagonal basis $\{f_g; n\}$ of the model

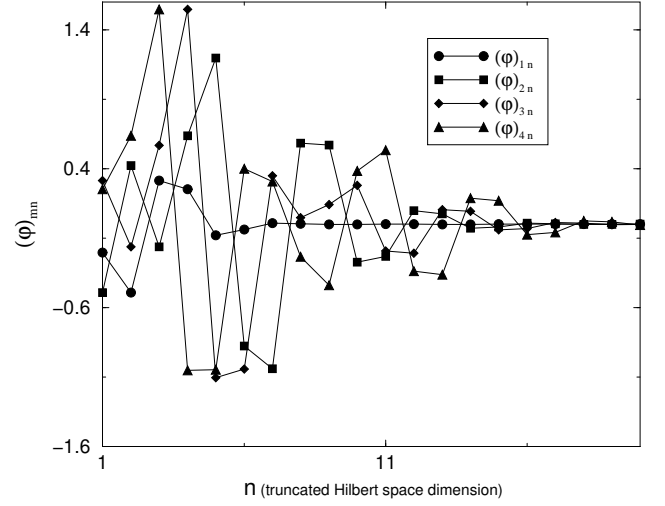


FIG. 3: A few non-zero dipole matrix elements $(z)_{nm}$ of the coupling of the rf-SQUID to a flux noise versus the truncated Hilbert space dimension [calculated in the eigenenergy basis of (1)]

system the interaction Hamiltonian is given by

$$H_{int} = \frac{\gamma}{2} \sum_{r,s=0}^{N-1} (z)_{rs} \phi_e |f_r\rangle \langle f_s| \quad (3)$$

Here $(z)_{rs} = \langle f_r | z | f_s \rangle$ are the noise induced perturbative dipole matrix elements of the macroscopic system coordinate z in the MLS's diagonal basis in (2). For the model MLS described by (1), the dipole matrix elements are real and symmetric.

The rf-SQUID poses a general example in which the multilevelledness of the master system manifests itself by finite dipole transition matrix elements for both the symmetric (i.e. $\gamma_{bias} = 0$) and asymmetric (i.e. $\gamma_{bias} \neq 0$) potential configurations. In the symmetric contribution even parity transitions vanish which results in manifestly off-diagonal system-noise coupling. Physically, this is in contrast to the most popular models used in the literature. On the other hand, when the potential is tilted, the parity selection no more holds by which finite diagonal couplings are also created.

In Fig. 3 the noise induced couplings for an asymmetric potential is plotted as a function of the truncated Hilbert space dimension. Data indicate that the induced dipole strengths between the qubit and the higher energy states are comparable to those among the qubit states. Therefore, the high energy transitions cannot be trivially ignored. The high energy transitions normally appear as a result of resonant interactions with the high energy sector of the noise spectrum under long interaction times. However, in the reduced system these transitions appear in the short time dynamics as well, and the short time dynamics is dominated by the nonresonant processes. Considering that decoherence is dominantly affected by the short time behaviour, the nonresonant

processes are expected to have observable effects in the decoherence properties of the RDM. Indeed we observe these effects in the solution of the master equation for the MLS (section IIIB and C).

The next is to consider the environmental spectrum and the availability of the bath frequencies for these excitations. Regarding this, we consider a thermal Gaussian environmental spectrum

$$I(\omega) = \omega^{1+\nu} e^{-\omega^2/4T^2} \coth(\omega/2T) \quad (4)$$

where ω is the effective noise cutoff frequency and ν describes the subohmic (i.e. $\nu < 0$), superohmic (i.e. $\nu > 0$), and ohmic (i.e. $\nu = 0$) character of the spectrum. The three environmental parameters ω , ν , T determine the sectors of the spectrum where the system-noise coupling is most effective. For $\omega \ll T$ (extreme subohmic), two regions are of particular importance: a) at sufficiently low temperatures and high cutoff corresponding to $T/\omega \gg 1$, the dominant mechanism of relaxation is through spontaneous deexcitations⁸. We call this region region-I; b) at high temperatures and high cutoff the region $0 < \omega/T \ll 1$ provides a wider range of strong environmental couplings which we call as region-II. If the character of the spectrum is more like ohmic or superohmic, i.e. $\nu \approx 0$ or $\nu \approx 1$ respectively, there is lesser room for deexcitations as the availability of the low energy modes is suppressed. Therefore, in the ohmic and superohmic regimes, the region-II dominates the RD phenomena.

Another feature of (4) is related to the majority of critical crossover behaviour in the vicinity of $\omega = 0$ as predicted earlier by Leggett et al. and depicted in Fig.4. In this figure, the $\omega = 0$ is a critical vicinity in the Ohmic region separating the subohmic $\nu < 0$ regime from that $0 < \nu$. In the subohmic regime $I(\omega) = (2T)^{1+\nu}$ is very small except for vanishingly small frequencies ($\omega = 2T$). Whereas, in the regime $0 < \nu$ the maximum value of $I(\omega)$ is observed at higher frequencies $\omega \approx 2T^{1/(1+\nu)}$ with an intensity proportional to $(\omega/2T)^{1+\nu}$.

III. MASTER EQUATION AND THE REDUCED DENSITY MATRIX FOR THE MLS

In the study of decoherence effects due to the weak environmental influences, one conventional way is to calculate the time dependent RDM elements by solving the master equation. This formalism has been known since the independent works of Bloch, Redfield and Fano (BRF)⁹ on spin-boson magnetic resonance and widely applied to the spin-boson systems for which many standard references exist¹⁰. The standard BRF formalism assumes Markov conditions for the solution of the master equations, which leads to exactly solvable results for 2LS¹¹. However, the Markovian assumption is not free of drawbacks and that was questioned originally in¹² and lately in¹³ as well as¹⁴ in the context of spin magnetic resonance and relaxation.

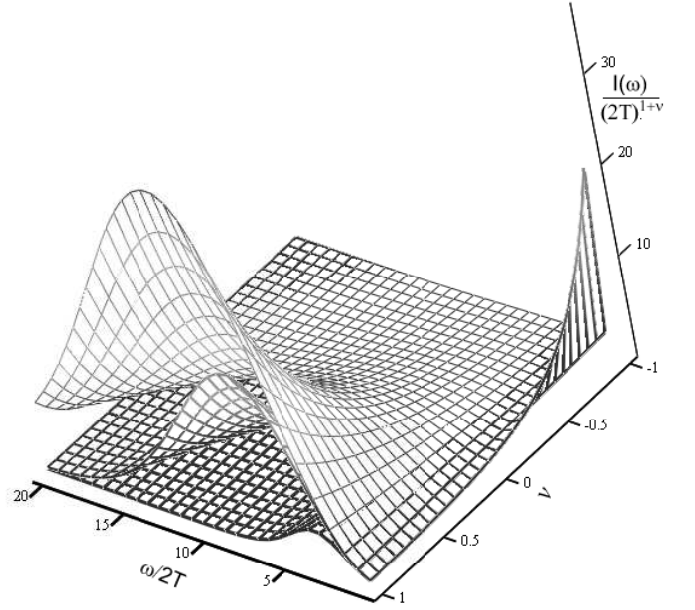


FIG. 4: The variation of $I(\omega)$ in (4) versus ω and T for $\nu = 10; 50; 100$ (from the innermost to the outermost surfaces respectively).

In this work, the system noise kernel is treated with its most general non-Markovian character¹⁵. The time evolution of the RDM is obtained in the interaction representation by

$$i\hbar \frac{d}{dt} \hat{\rho}(t) = [\hat{\rho}(t); H_{int}(t)] \quad (5)$$

where \sim denotes the interaction picture. In the context of decoherence, we will give more emphasis on short observational times in the solution of (5). A convenient way to proceed is then to apply the Born approximation in which the full density matrix is initially a product of the system and environmental ones (i.e. $\hat{\rho}(0) = \hat{\rho}^{(s)}(0) \hat{\rho}^{(n)}(0)$) and at any later and short time approximately separates as $\hat{\rho}(t) = \hat{\rho}^{(s)}(t) \hat{\rho}^{(n)}(0)$.

The exact iterative solution of (5) including the second order in the interaction with the partial trace performed over the environmental degrees of freedom yields for the RDM the integro-differential equation

$$\frac{d}{dt} \hat{\rho}_{nm}^{(s)}(t) = \int_0^t dt' \sum_{r,s} K_{rs}^{nm}(t; t') \hat{\rho}_{rs}^{(s)}(t') \quad (6)$$

in which we adopt the model interaction Hamiltonian (3) for the system-noise kernel which is found to be

$$K_{rs}^{nm}(t; t') = \frac{1}{4} F(t-t') [(\hat{z}_t \hat{z}_{t'})_{nr} (\hat{z}_{t'} \hat{z}_t)_{sm}] + F(t-t') [(\hat{z}_{t'} \hat{z}_t)_{ms} (\hat{z}_t \hat{z}_{t'})_{nr}] \quad (7)$$

Note that the kernel depends on two times as a signature of the non-Markovian treatment and it is not time translationally invariant. Here $F(t-t') = F(t' - t)$ is the

complex noise correlation function

$$F(t, t') = \text{Tr}_n \hat{\rho}_n^{(n)}(t) \hat{\rho}_n^{(n)}(t') \quad (8)$$

$$= \text{Tr}_n \hat{\rho}_n^{(n)}(t) \hat{\rho}_n^{(n)}(t')$$

and

$$\hat{z}_t = \sum_{k,j} (z_k)_j e^{i(E_k - E_j)t} \hat{z}_{kj} \quad (9)$$

is the time dependent dipole operator in the interaction picture where $E_k; j$ comprise the eigensolution of the model system. Expanding the noise field \hat{E}_e in the independent harmonic modes and calculating (8) in thermal equilibrium one obtains the standard thermal noise correlator

$$F(t, t') = 2 \sum_k \left[\coth(\beta \hbar \omega_k / 2) \cos \omega_k(t - t') \text{Re} \hat{z}_k(t) \hat{z}_k(t') + i \sin \omega_k(t - t') \text{Im} \hat{z}_k(t) \hat{z}_k(t') \right] \quad (10)$$

The Markovian versus non Markovian character of the solution of (6) is determined in the weak system-noise interaction limit by the competition of three time scales: τ_B , noise correlation time scale, τ_R and τ_{dep} , the relaxation and dephasing time scales¹⁶ of the reduced system respectively. The noise correlation time scale is found roughly from the thermal Gaussian bath spectral width as $\tau_B^{-1} = \sum_k \omega_k^2$. At the Markovian limit, the environmental correlation time τ_B^{-1} is much smaller than the RD times. For two level systems this condition can be met provided that the system noise-coupling is sufficiently small. However, for MLS, the question of whether the Markovian condition is satisfied is more nontrivial. The basic reason is that in the MLS there is a larger number of time scales and decay channels of which presence may considerably reduce the effective decoherence times.

In this work, the numerical solution of (6) is performed by discretizing time in steps $\Delta t = 10^{-2}$. The Hermiticity and the normalization of the RDM at each time step is maintained within an accuracy of 10^{-25} .

A. The system-noise Kernel

In the model Hamiltonian defined in (1) all energies and time scales (particularly the RD times) are given in units of $\hbar \omega_0$ and ω_0^{-1} respectively. The parameters affecting the numerical results are, $\beta; T$ for the thermal noise, γ for the system-noise bare coupling and the dipole matrix elements $(z)_{nm}$ for the pure MLS. The noise spectrum is assumed to be continuous of which the real part is responsible for RD effects and is given by the spectral density in (4). In the Markovian limit the imaginary part of $F(t, t')$ is vanishingly small and the resulting Lamb-type energy renormalization effects are negligible. In the numerical calculations however we include the full complex noise correlation function as¹⁷

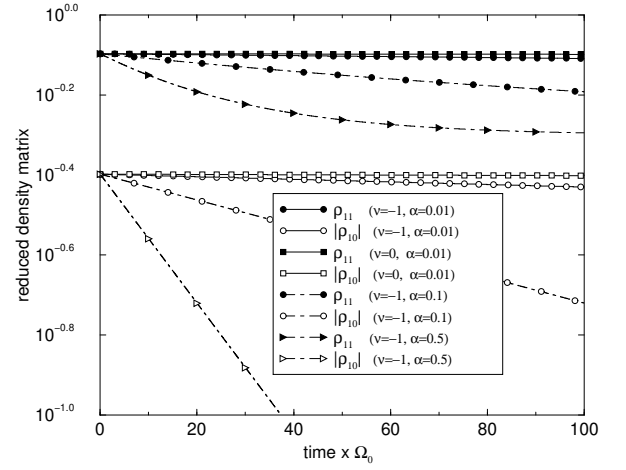


FIG. 5: Time dependence of the RDM in units of ω_0^{-1} for various representative parameter sets at $T = 0$ and $\gamma = 0.1$. For the model system the potential is symmetric and the bare TLS is in SD conjugation.

$$F(t, t') = 2 \sum_k \left[\coth(\beta \hbar \omega_k / 2) \cos \omega_k(t - t') \text{Re} \hat{z}_k(t) \hat{z}_k(t') + i \sin \omega_k(t - t') \text{Im} \hat{z}_k(t) \hat{z}_k(t') \right] \quad (11)$$

Inserting (11) in (7) we obtain the system-noise kernel for our model. An upper frequency cutoff $\omega_{\text{max}} = 5$ is used in the numerical integral in (11).

B. Overview of the 2LS results

We now examine the time behaviour of the RDM in (6) for a 2LS. The solution is shown in Fig. 5 on the logarithmic scale for a few representative parameters and for the SD conjugation. The degeneracy parameter is $\gamma = 10^6$. We also fixed $\beta = 0.01$ in the rest of the work unless otherwise stated.

In Fig. (5) the first observation is that, exponential RD is effective immediately in the short time regime $t < 20 \omega_0^{-1}$. We also confirmed numerically that the asymptotic time behaviour as well as the RD rates are independent of the initially prepared state. As the asymptotic time behaviour is concerned, for symmetric conjugations (pure \times coupling), the density matrix converges to the maximum entropy (informationless) limit $\hat{\rho} = \hat{I}/2$, where \hat{I} is the unit matrix, irrespectively from the spectral properties of the noise or the system-noise coupling. The results also indicate that the relaxation time scale τ_R (read from the filled symbols) and the dephasing time scale τ_{dep} (read from the hollow symbols) are compatible. This result is in agreement particularly with the recent exact 2LS calculations using the path integral in influence functional formalism⁴.

We also confirm that all regions in the noise spectrum have strong influence on RD. For this observation,

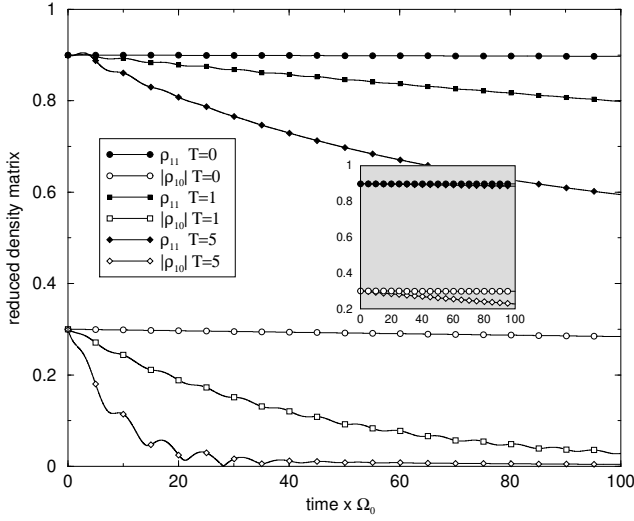


FIG. 6: Time dependence of the RDM when the system potential is biased by $V_{\text{bias}} = 0.2$. The other parameters are $\gamma = 0.01$; $\beta = 0.1$ and $\Omega = 1$. Comparing this figure with the previous one, a crossover in the time dependence of the RDM is observed in the T plane. The $\gamma = 0$ data is also added in the inset to facilitate this comparison.

one has to compare Fig's. 5-9 corresponding to different spectral properties and temperatures. For instance, for $\gamma = 0.01$; $\beta = 0.1$ and $T = 0$ [see Fig.5], we recover the underdamped and weak dephasing limit of ρ^2 for all Ω . In addition, no oscillations are observed in the SD configuration.

Larger RD rates are observed as Ω is made to be more negative towards $\Omega = 1$. We identify this behaviour as the manifestation of the region-II in the noise spectrum (see the end of section IIA). More data are also shown in the same figure for indicating the effect of various values. In Fig.6 the nondegenerate case with an energy difference between the levels $E = 1.2\hbar\Omega_0$ is shown for $\gamma = 0.01$; $\beta = 1$; $\Omega = 0.1$ and for various temperatures. The $\gamma = 0$ and $\beta = 1$ curves again yield weaker RD rates within the indicated temperature ranges. Another noticeable feature in Fig.6 is the weakly oscillating behaviour. The weak oscillations are more prominent at high temperatures and short times. In this case for $\Omega > T$ the system-noise coupling is large due to the large number of thermally activated environmental modes. This behaviour, which is characterized by weakly damped Rabi-like oscillations, was predicted in the analytic calculations of Leggett et al. In order to examine the influence of the spectral width a similar zero temperature plot as in Fig.5 is made in Fig.7 for a wider spectral width $\Omega = 1$. Comparing this figure with Fig.5, a crossover in the time dependence of the RDM can be observed in the T plane. (The crossover can also be activated thermally as to be seen in the following Fig's 8 and 9.)

There are a number of ways to increase the effective system-noise coupling. The following Fig.8 gives a sam-

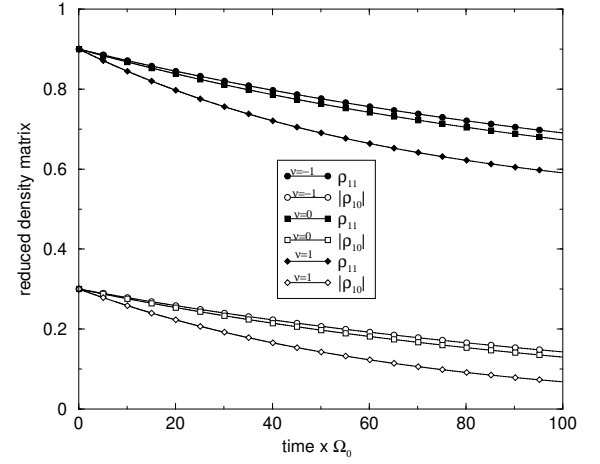


FIG. 7: Time dependence of the RDM in the SD configuration. The other parameters are fixed at $T = 0$, $\beta = 0.1$ and $\Omega = 1$.

ple from the T behaviour for the asymmetric potential configuration. Increasing the temperature increases the coupling by filling the available photon modes for $\Omega < T$. The sample data is shown for $T = 0; 1; 5$ at $\gamma = 0.01$; $\beta = 5$ and $\Omega = 1$ (indicated by the filled and opaque symbols connected with solid lines). The second way to increase the system-noise coupling is to directly increase Ω (indicated by the dotted dashed lines). In the small coupling regime, for which the sample data is shown for $\gamma = 5 \cdot 10^{-4}; 10^{-2}; 5 \cdot 10^{-2}$ at $T = 0$ $\beta = 1$ and for an increased Ω ($\Omega = 5$), the RDM experiences stronger damping. The weakly damped oscillations survive at short times at finite and small temperatures. The larger the temperature the larger the amplitude of the oscillations and the faster they diminish.

For completeness we also add in Fig.9 the behaviour in the T plane at zero temperature. A comparison between the Fig's 8 and 9 reveals a temperature modulated crossover (compare, for instance, a similar decay of the sets for $\gamma = 5$; $\beta = 1$ at $T = 5$ in Fig.8 with $\gamma = 5$; $\beta = 1$ at $T = 0$ in Fig.9).

Then a major difference of the model interaction Hamiltonian in (3) from the standard (σ_z -type) spin-boson model is in the manipulation of the potential. In contrast to the standard spin-boson model, in our case only non-diagonal, σ_x , type coupling is present under the symmetric potential [see Fig.3]. As a result, dramatic differences in the time dependence of the reduced system are observed between the two models. For instance, the diagonal coupling is standardly considered for the study of pure dephasing. In this type of coupling the relaxation is manifestly forbidden and the initial states do not change their populations. The diagonal coupling also yields strongly temperature dependent dephasing rates with the rates vanishing at $T = 0$. On the other hand, when the system-noise coupling is not diagonal, the induced transitions between the system states

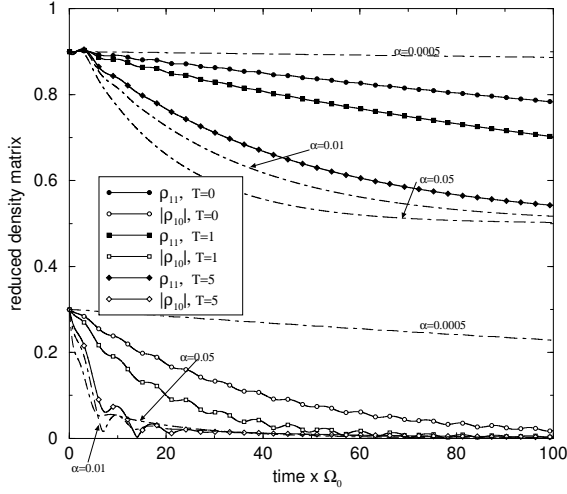


FIG. 8: The T behaviour of the RDM is shown for an asymmetric potential with $V_{\text{bias}} = 0.2$. The noise parameters are $\omega = 10^{-2}$, $\gamma = 5$ and $\eta = 1$.

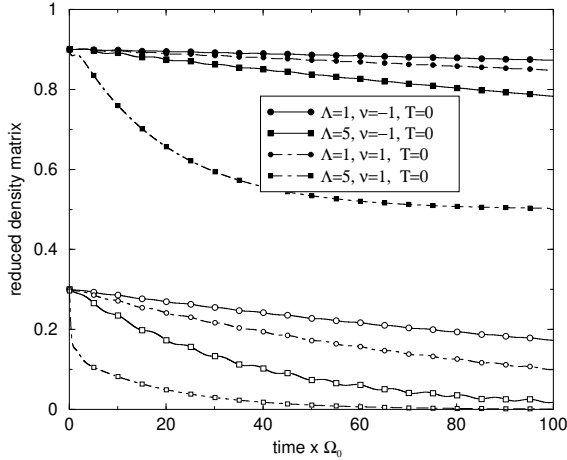


FIG. 9: The density matrix parameterized by different λ and ν values at $T = 0$ and $\alpha = 0.01$ for the asymmetric potential with $V_{\text{bias}} = 0.2$. The crossover from the weakly oscillating damped behaviour at short times to strong relaxation at longer times can be observed.

can probe the entire noise spectrum creating decoherence even at zero temperature. These induced transitions are nonresonant and they have observable effects particularly in the short time dynamics of the RDM¹⁸. The RD times observed as the result of such system-noise coupling are expected to be nonzero even at zero temperature. This characteristic behaviour of the non-diagonal coupling is confirmed in our calculations both for the 2LS in Figs. 5-9 and for the MLS in the following sections. Recently, there are other claims using realistic models on decoherence effects in mesoscopic systems¹⁹ as well as a few experimental confirmations on the saturation of the RD rates at low temperatures²⁰.

A curious observation in Fig's 5-9 is the strong de-

pendence of RD time scales on the spectral width. A naive expectation is that for E and at very small temperatures the resonant transitions are unfavoured and there are no environmental modes available therefore the relaxation should be inhibited. The point that is often missed in this popular argument is the different role played by the short time nonresonant transitions. The resonant transitions are favoured when the system interacts with the environment at sufficiently large times. The system however relaxes differently at short times by preferring to stay off-resonant in its interaction with the noise field thereby sampling all regions of the noise spectrum. This causes the strong dependence on ω we observe at short times.

In summary, it is confirmed that the rich transient effects are observed usually in the short time behaviour in which all energy scales in the noise spectrum take part rendering the relaxation process sensitive to the relative magnitudes of those scales. We confirmed the several crossover regions that have been predicted in the path integral influence functional calculations.

The decoherence and dephasing dynamics is governed by all frequency regions in the noise spectrum. In particular, the short time behaviour is affected strongly by all frequency regions due to the nonresonant processes. For $\omega = 1$, Fig. 5 indicates that as α increases in the interval 10^{-2} to 10^{-1} the relaxation rates gradually increase still remaining in the weak relaxation regime. A crossover in the α - T plane is observed [compare with Fig. 7] as ω is increased. With this being the case for symmetric potentials, for asymmetric ones the additional feature of weak oscillations are present in the short time dynamics.

C. MLS with 3 N

The effect of multilevelness on decoherence has not yet received the attention that it deserves in the literature. This is, in part, due to the lack of practical analytic tools in solving the master equation. The complexity of the formal methods such as the noninteracting blip approximation increases at each time step as N^2 which renders the analytic sum over all virtual configurations in the path integral approach intractable. Usually, the common argument is that, for sufficiently low temperatures, a multilevel system, of which the first two levels (the qubit) are sufficiently well separated from the rest, behaves as a two state system. We have already observed that there are two major pitfalls in this assumption. Firstly, it excludes the very realistic case in which decohering effects are induced through interactions with a strongly fluctuating quantum field. In such a case, the fluctuations in the distribution of environmental modes in the noise spectrum is the major source of decoherence. Secondly, and more generally, the short time behaviour of a MLS—which is the most prominent regime in the quantum computational perspective—is affected by a large frequency region in the noise spectrum. These comprise the basic motiva-

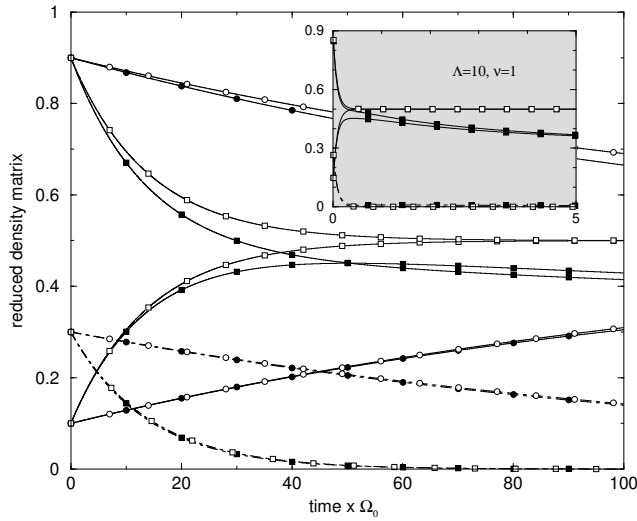


FIG. 10: Comparison of the effect of the spectral width on the time dependence of the elements ρ_{00} , ρ_{11} and ρ_{01} between the 2LS and 3LS. The fixed parameters are $T = 0$, $\gamma = 0.01$ and $\lambda = 1$. The open symbols refer to the case $N = 2$ and the solid ones refer to $N = 3$. Also the solid lines are the diagonal elements ρ_{00} (with $\rho_{00}(0) = 0.1$) and ρ_{11} (with $\rho_{11}(0) = 0.9$), the dotted-dashed lines are the non-diagonal ones ρ_{01} (with $\rho_{01}(0) = 0.3$). More specifically, circle is $\lambda = 1$, square is $\lambda = 10$. The inset is the case $\lambda = 1$ and only $\lambda = 10$ is displayed for simplicity.

tion of why we should look into the effect of higher levels on decoherence in a MLS. We will continue by examining the cases $N = 3$ and $3 < N$ separately. In particular, we remark on certain interesting decoherence properties of the doubly degenerate systems with $4 \leq N$.

$N = 3$ case

From the quantum computational point of view, the three level systems are as important as the two level ones (see for instance²¹). Recently, the Linblad approach was used for the RDM of a multilevel system in connection with the quantum Zeno effect²². The Linblad equation is derived directly from the Bloch-Redfield-Fano equation for the RDM and is based on the validity of the Markovian condition¹. We compare in Fig.10 the solutions of the RDM for $N = 2$ and $N = 3$ at $\gamma = 0.01$, $T = 0$ and for $\lambda = 1; 10$. We look at the symmetric potential in the SD configuration. For 3LS, the observed energies form a λ -shaped configuration and, in units of ϵ_0 , are roughly $E_0 \approx E_1 \approx 0.1$ and $E_2 \approx 2.3$. The degeneracy parameter $\lambda = (E_2 - E_1) = (E_1 - E_0) \approx 10^6$ and the third level E_2 is above the double well barrier as shown in Fig. (1). Here we mainly discuss the subohmic case $\lambda = 1$.

When $\lambda = 1$ the resonant coupling of the first two levels to the third level is very weak. In principle, at short observational times, the nonresonant excitations are induced with frequencies much higher than the resonant frequency $E_3 - E_2 \approx 2$ (in units of ϵ_0). When $\lambda = 10$

however, these transitions are suppressed by the Gaussian cutoff. As a result, the 3LS is basically confined to its highly degenerate qubit subspace. This confinement can be observed all the way up to much higher spectral widths such as $\lambda = 10$ as long as the Gaussian suppression is manifested. This behaviour is shown in Fig.10 for $\lambda = 1$ and $\lambda = 10$. For considerably long duration (i.e. $100 \epsilon_0^{-1}$) and for $\lambda = 1$ the qubit subspace in the three level system has a negligible leakage into the third level. For much larger λ such as $\lambda = 10$, the third level is allowed to participate in the transitions. The RD rates are therefore found to be significantly larger than that of the $N = 2$ case before.

An enhancement in the high frequency and suppression in the low frequency coupling as compared to $\lambda = 1$, is generated if we now consider $\lambda = 1$ (shown in the inset of Fig.10). Under these conditions, the short time behaviour is dramatically influenced by a strong leakage to the third level (note the short time span on the horizontal axis between zero and $5 \epsilon_0^{-1}$).

The asymptotically long time dynamics is independent of the system-noise parameters. In sufficiently long time the system loses all the information that is put in the initial state: $\rho_{kk}(t \rightarrow \infty) = 1/3$; ($k = 0; 1; 2$) and $\rho_{kj}(t \rightarrow \infty) = 0$; ($k \neq j$).

$N = 4$ case

We compare the 4LS with a 2LS in Fig.11 for $\lambda = 1$. Here, we have three sets of curves indicated by (a), (b) and (c). In Fig.11a the 4LS is compared to 2LS when both systems are highly degenerate. In Fig.11b the four level system is doubly degenerate and at zero temperature. The third set of curves are plotted in Fig.11c corresponding to the DD configuration at finite temperatures.

For the singly degenerate (SD) case, the qualitative features between the 2LS and the 4LS are similar to the previously discussed case between 2LS and the 3LS. Here, we observe for the diagonal elements, a much higher relaxation rate (as well as leakage) out of the qubit subspace during the observed time although the dephasing rates are indistinguishable for the 2LS and the 4LS. The RDM asymptotically approaches to the informationless limit $\hat{\rho} = \hat{I}/4$.

For $N = 4$ we have the chance to look at the DD configuration as depicted in Fig. (2). For the doubly degenerate configuration, the degeneracies are as high as $\lambda_2 = (E_2 - E_1) = (E_1 - E_0) \approx 3 \cdot 10^6$ and $\lambda_1 = (E_3 - E_2) = (E_2 - E_1) \approx 10^6$. We surprisingly observe a tremendous suppression (by almost two orders of magnitude) at sufficiently small temperatures in the RD rates (Fig.11b). The rates and the DD-suppression strongly depend on the temperature. A comparison of the $T = 0$; $\lambda = 1$ in Fig.11b and $T = 1$; $\lambda = 1$ in Fig.11c can reveal this strong dependence.

$4 < N$ case

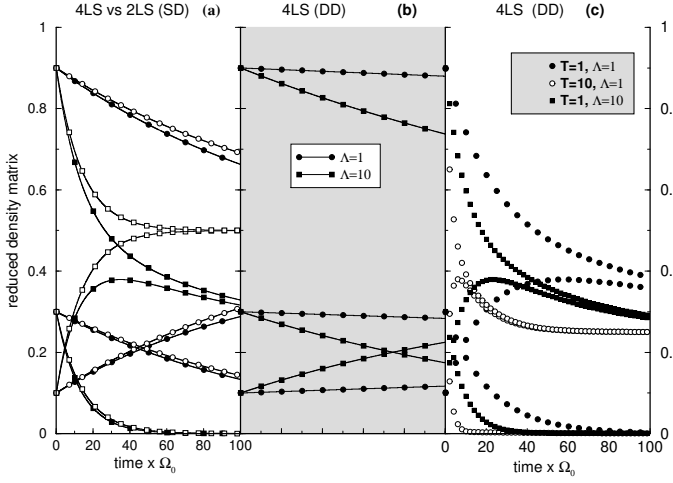


FIG. 11: (a) Comparison, at $T = 0$ and $\Lambda = 1$, of the effect of the spectral width on the time dependence of the elements ρ_{00} , ρ_{11} and ρ_{01} between the 2LS and 4LS. The symbols are the same as in Fig.10. The figure describes the singly degenerate case $\Gamma = 10^6$; (b) the rates at $T = 0$ and $\Lambda = 1$ for the doubly degenerate (denoted by DD in the figure title) configuration $\mathbf{E}_2 = (\mathbf{E}_2, \mathbf{E}_1) = \mathbf{E}_1, \mathbf{E}_0)^T$ 3×10^6 and $\mathbf{E}_1 = (\mathbf{E}_3, \mathbf{E}_2) = \mathbf{E}_2, \mathbf{E}_1)^T$ 10^6 [horizontal and vertical axes have the same span as (a)]; (c) the thermal case at the indicated T values at $\Lambda = 1$.

In order to extract some quantitative numbers for the RD times we made use of the numerical observation that for weak system-environment coupling the time dependence is approximately exponential at short times. We then follow³ and write for the time dependence of a general matrix element at short times

$$\rho_{ij}(t) \approx \rho_{ij}(1) + [\rho_{ij}(0) - \rho_{ij}(1)] \exp(-t/\tau_{ij}) \quad (12)$$

The RD times are extracted from the time dependence of $\rho_{11}(t)$ and $\rho_{10}(t)$ respectively as

$$\tau_{ij}^{-1} = \frac{1}{1 - \rho_{ij}(1) - \rho_{ij}(0)} \frac{d \ln \rho_{ij}}{dt} \bigg|_{t=0} \quad (13)$$

where $i = j = 1$ is used in the calculation of the relaxation rate and $i = 0; j = 1$ is for the qubit dephasing rate corresponding to the first excited level. For the RDM at asymptotic times we have $\rho_{11}(1) = 1/N$ and $\rho_{10}(1) = 0$. The equation (13) breaks down when $\rho_{ij}(0) = \rho_{ij}(1)$ which we stay away by appropriately choosing $\rho_{ij}(0)$. In Fig.12 the data are represented at zero temperature and $\Lambda = 0$. To be used in (13), the initial conditions are set at $\rho_{00}(0) = 0.2$; $\rho_{11}(0) = 0.8$; $\rho_{10}(0) = 0.4i$ with all density matrix elements outside the qubit subspace zero. Three different curves stand for (bottom to top) $\Lambda = 0.1; 1; 10$ with the open symbols corresponding to dephasing and the solid ones to the relaxation rates. Each set of data is shown for SD as well as DD configurations separately. Also note that the vertical axis is logarithmic.

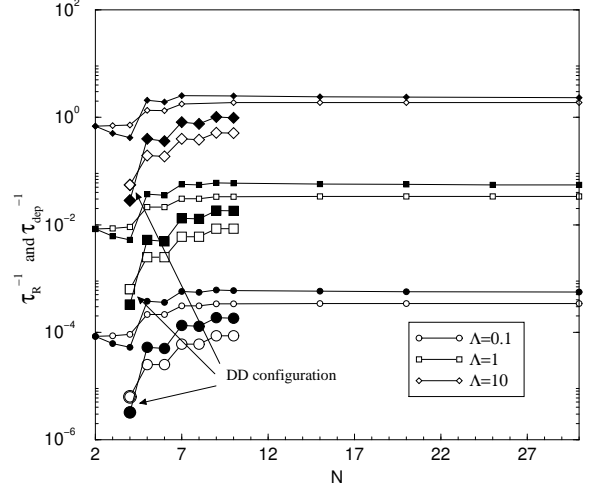


FIG. 12: Relaxation and dephasing rates against the number of levels for different spectral widths at $T = 0$ and $\Lambda = 0$. Note the logarithmic vertical axis. Small symbols refer to the singly degenerate MLS and the larger symbols refer to doubly degenerate one. The open and solid symbols refer to dephasing and relaxation times respectively.

Let us concentrate first on the SD configurations in Fig.12. In a large range $N = 4$ and $N = 10$ appear to be two crucial points. For $4 < N$ relaxation is approximately twice faster than dephasing and both rates rapidly saturate near $N = 10$ and they are independent of N for $10 < N$. The onset of saturation is naturally model dependent. In our case this onset coincides with the range of strong dipole transition matrix elements of the model in (1) (see Fig.3). Turning to the DD configurations, we observe that for the same environmental parameters and for all N , decoherence rates for the DD case are strongly suppressed by nearly two orders of magnitude as compared to the SD configuration.

With this section we conclude the RD calculations for the interaction between the system and the thermally equilibrated noise. We now focus our attention on the calculations of the transition rates by a different approach, the Fermi Golden rule.

IV. FERMIGOLDEN RULE

The Fermi Golden Rule (FGR) provides a simple and qualitative tool to reproduce many of the features of the relaxation times that we observe in Fig.12. Quantitative agreement should not be expected between the Fig.12 and the FGR results. This is mainly due to the fact that the data produced in Fig.12 reflects the effects of the short time dynamics whereas, the FGR gives more accurate results for the long time resonant interactions. In comparing the time scales found by directly solving the RDM and by FGR, we keep the absolute time scales arbitrary and only compare the qualitative behaviour.

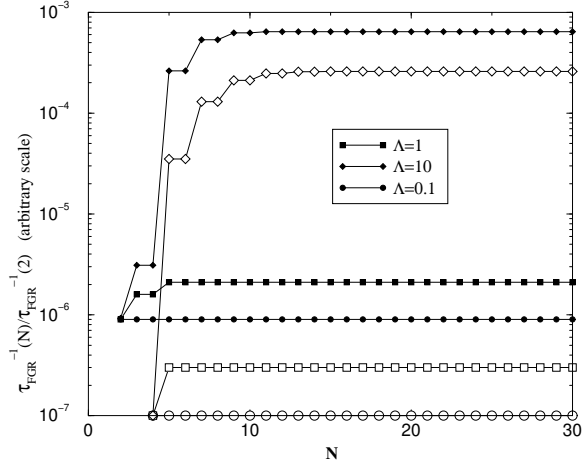


FIG. 13: Relaxation rates against the number of levels for the SD (solid symbols) and DD (open symbols) cases.

We assume that the MLS is prepared at $t = 0$ in the first excited state $|f; g; 1\rangle$. The probability that the system stays in the same state after interacting with the environment for a duration t is³

$$p(t) = \langle h(0) | \exp\left[-\frac{i}{\hbar} \int_0^t dt H_{\text{int}}(t^0)\right] | j(0) \rangle^2 \quad (14)$$

where for our case $|j(0)\rangle = |f; g; 1\rangle$. Including second order perturbation in the dipole couplings with an environment in thermal equilibrium, (14) can be written as

$$p(t) = \frac{1}{2} \left(\frac{1}{2} \right)^2 \sum_s \left(\frac{1}{2} \right)^2 \int_0^t dt^0 \int_0^{t^0} dt^{\infty} e^{i(E_{n_0} - E_s)(t^0 - t^{\infty})} F(t^0 - t^{\infty}) \quad (15)$$

where $F(t^0 - t^{\infty})$ is the environmental correlation function given by (10). The relaxation rate τ_{FGR}^{-1} corresponding to the first excited state is found by the same method that is described in (3) [The Eq. (3.37) therein].

The relaxation times found by the FGR are summarized in Figs 13, and 14. In Fig. 13 the relaxation times are plotted against the same parameters as in Fig. 12 with the same symbols. The FGR data reproduce many of the features in Fig. 12. The first observation is the same onset at $N = 4$ and the saturation of the rates slightly above this onset with a rapid increase for $4 < N$. The second observation is that by increasing the spectral width, the relaxation rates can be increased by as much as an order of magnitude.

When the temperature is varied, we observe the same trend as in the previous figure as depicted in Fig. (14).

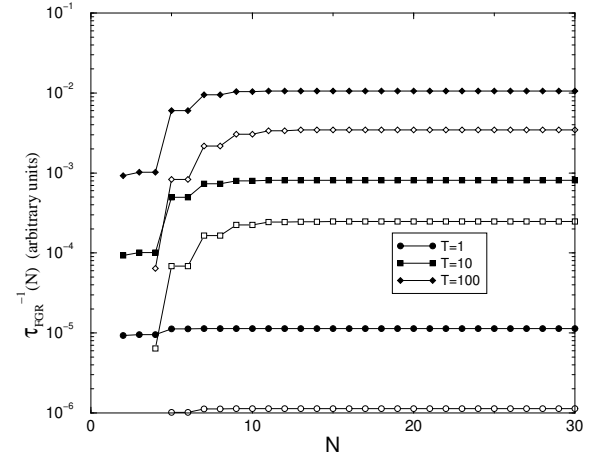


FIG. 14: Comparison of the absolute relaxation rates (in common arbitrary units) with N between the SD (solid symbols) and DD (open symbols) durations. Here, $\omega = 0$ and $\omega_s = 10$. Same temperatures are implied for each SD-DD pair.

V. CONCLUSIONS

We examined the RD properties of a multilevel system using non-Markovian master equation formalism. It is shown that the short time behaviour of the density matrix is influenced by nonresonant transitions in the MLS receiving contributions from all frequency regions in the noise spectrum. For the model interaction used, the dipole transitions are nonzero within a finite range of levels. The RD times calculated within this model show a saturation within the same range largely independent from the system-noise parameters.

It is generally found that the decoherence effects in MLS are more pronounced than those in the 2LS. We observe that a distinct counter example is posed by the doubly degenerate MLS with $4 \leq N$. The RD rates are found to be highly suppressed in comparison with the singly degenerate or non-degenerate systems for the same system and environment parameters. These results were also confirmed using the transition rates found from the Fermi-Golden rule. At the first glance, this curious suppression of decoherence reminds us the decoherence free subspaces. Nevertheless, the arbitrariness of the parameters of the DD model, and in particular of the dipole matrix elements rules out the possibility whether any set of invariant states can form a decoherence free subspace under the coupling with the environment. In order to understand the true nature of this strong suppression, more formal and analytic methods must be developed for the DD system S^2 .

VI. ACKNOWLEDGEMENTS

This research is supported by the Scientific and Techni-
cal Research Council of Turkey (TUBITAK) grant num -

ber TBAG-2111 (101T136). The authors thank IO Kulik
and E Mese for comments.

-
- ¹ A.O. Caldeira and A.J. Leggett, Phys. Rev. Lett. 46, 211 (1981); A.O. Caldeira and A.J. Leggett, Annals of Physics 149, 374 (1983).
- ² A.J. Leggett and Anupam Garg, Phys. Rev. Lett., 54, 857 (1985).
- ³ A.J. Leggett, S. Chakravarty, A.T. Dorsey, Matthew P.A. Fisher, Anupam Garg and W. Zwerger, Rev. Mod. Phys. 59, 1 (1987); Daniel Loss and David P. DiVincenzo, Exact Born Approximation for the spin-boson model, [cond-mat/0304118]; Till Vorrath, Tobias Brandes Bernhard Kramer, Dynamics of a large spin-boson system in the strong coupling regime, [cond-mat/0111220].
- ⁴ Charis Anastopoulos and B.L. Hu, Phys. Rev. A 62, 033821 (2000).
- ⁵ M. Dube and P.C.E. Stamp, Mechanism of Decoherence at Low Temperatures, Chem. Phys. Quantum Physics of Open Systems, Special Issue (2001) also [cond-mat/0102156]; P.C.E. Stamp, I.S. Tupitsyn, Crossovers in spin-boson and central spin models, [cond-mat/0308139]; Leonid Fedichkin, Akhady Fedorov and Vladimir Pirmian, Measures of Decoherence [cond-mat/0303158].
- ⁶ Lin Tian and Seth Lloyd, Phys. Rev. A 62, 050301 (2000).
- ⁷ In a finite double well potential there is no manifest degeneracy. However highly degenerate configurations can be obtained in the vicinity of level crossings. It can be numerically shown [see for instance T. Hakioglu, J. Anderson, F. Wellstood, Phys. Rev. B 66, 115324 (2002)] that at the level crossings the symmetric and antisymmetric configurations are highly correlated either within the left or the right wells. The tunneling matrix element is proportional to the overlap of these configurations which is minimized at the level crossings.
- ⁸ We assume that the system is initially prepared at a given superposition state $|0\rangle = a|\downarrow\rangle + b|\uparrow\rangle$ where $|\downarrow\rangle$ and $|\uparrow\rangle$ are respectively the ground and the first excited states in the qubit subspace.
- ⁹ F. Bloch, Phys. Rev. 102, 104 (1956); A.G. Redfield, IBM J. Res. Develop. 1, 19 (1957); U. Fano, Phys. Rev. 96, 869 (1954).
- ¹⁰ Michele G. Overmalle, Milena G. Rifoni and Gerd Schon, Chem. Phys. 208 273 (2001); Guido Burkard, Roger H. Koch and David P. DiVincenzo, Multilevel quantum description of decoherence in superconducting flux qubits [cond-mat/0308025]; Yuriy Makhlin, Gerd Schon and Alexander Shnirman, Dissipation in Josephson Qubits, [cond-mat/0309049].
- ¹¹ Anatoly Yu. Smirnov, Phys. Rev. B 67, 155104 (2003); and the third reference in¹⁰.
- ¹² P.N. Agyres and P.L. Kelley, Phys. Rev. 134, 98 (1964).
- ¹³ A. Suarez, R. Silbey and I. Oppenheim, J. Chem. Phys. 97, 5101 (1992).
- ¹⁴ M. G. Rifoni, E. Paladino and U. Weiss, Eur. Phys. J. B 10, 719 (1999).
- ¹⁵ The Markovian versus non Markovian character of the system-noise kernel and the Markovian versus non Markovian character of the solution of the RDM should be clearly distinguished. In the former we take the most general form of the kernel as it comes out of the interacting model which depends on two times independently. The Markovian or non Markovian character of the solution however depends on whether the conditions B_R and B_{dep} are satisfied where B_R ; B_{dep} are the noise correlation, relaxation and dephasing time scales respectively. A good example of Markovian solution using a non Markovian kernel can be found in the last work in³ above.
- ¹⁶ H.P. Breuer and F. Petruccione, The Theory of Open Quantum Systems, Oxford Univ. Press, 2002.
- ¹⁷ B.L. Hu, Juan Pablo Paz and Yuhong Zhang, Phys. Rev. D, 45, 2843 (1992).
- ¹⁸ See for instance, a similar observation in other Aharonov-Bohm systems in Florian Marquardt and C. Bruder, Phys. Rev. B 65, 125315 (2002).
- ¹⁹ D.S. Golubev and A.D. Zaikin, Phys. Rev. Lett. 81, 1074 (1998); Phys. Rev. B 62, 14061 (2000).
- ²⁰ P. Mohanty, E.M.Q. Jariwala and R.A. Webb, Phys. Rev. Lett. 78 3366 (1997).
- ²¹ IO Kulik and T. Hakioglu, Eur. Phys. J. B 30, 219 (2002).
- ²² D. Brunno, P. Facchi, S. Longo, P. Minelli, S. Pascazio and A. Scardicchio, Quantum Zeno effect in a multilevel molecule, [quant-ph/0206143].
- ²³ T. Hakioglu, E. Mese and K. Savran, unpublished (2003).